Synthesis and Characterization of Intrinsic High-Barrier Polyimide Derived from a Novel Diamine Monomer Containing Rigid Planar Moiety

Yi-Wu Liu,[1,2] Jie Huang,[1] Jing-Hua Tan,[1] Yi Zeng,[1] Qian Ding,[1] Xian-Wei Xiang,[1] Yue-Jun Liu,[1] Hai-liang Zhang[2]

[1]Key Laboratory of Advanced Packaging Materials and Technology of Hunan Province, School of Packaging and Materials Engineering, Hunan University of Technology, Zhuzhou 412007, People's Republic of China
[2]Key Laboratory of Polymeric Materials and Application Technology of Hunan Province, Key Laboratory of Advanced Functional Polymer Materials of Colleges and Universities of Hunan Province, College of Chemistry, Xiangtan University, Xiangtan 411105, People's Republic of China
Correspondence to: J.-H. Tan (E-mail: tjh@hut.edu.cn)

Received 9 February 2017; accepted 7 April 2017; published online 3 May 2017
DOI: 10.1002/pola.28626

ABSTRACT: A new diamine monomer containing rigid planar fluorenone moiety, 2,7-bis(4-aminophenyl)-9H-fluoren-9-one, was synthesized through Suzuki coupling reaction. Then it was reacted with pyromellitic dianhydride to obtain a polyimide (FOPPI) via a conventional two-step polymerization process. The prepared FOPPI exhibits excellent barrier properties, with the oxygen transmission rate and water vapor transmission rate low to 3.2 $cm^3 \cdot m^{-2} \cdot day^{-1}$ and 2.9 $g \cdot m^{-2} \cdot day^{-1}$, respectively. The results of wide angle X-ray diffractograms, positron annihilation lifetime spectroscopy, and molecular dynamics simulations reveal that the excellent barrier properties of FOPPI are mainly ascribed to the crystallinity, high chain rigidity, and low free volume, which are resulted from the rigid planar moiety. FOPPI also shows outstanding thermal stability and mechanical properties with a glass transition temperature up to 420 °C, 5% loss temperature of 607 °C, coefficient of thermal expansion of 1.28 ppm K^{-1}, and tensile strength of 150.8 MPa. The polyimide has an attractive potential application prospect in the flexible electronics encapsulation area. © 2017 Wiley Periodicals, Inc. J. Polym. Sci., Part A: Polym. Chem. **2017**, *55*, 2373–2382

KEYWORDS: barrier; free volume; polyimides; rigid planar moiety; thermal properties

INTRODUCTION Flexible organic electronic devices (FEDs) such as flexible organic light emitting diodes (OLEDs) have attracted lots of attention over the past decade due to their portability and convenience.[1–3] In flexible OLEDs, the flexibility depends on the substrates.[4] Polymers are very promising substrate candidates for flexible displays. They offer the advantages of light weight, transparency, flexibility, even deformability, and compatibility with roll-to-roll manufacturing.[5,6] With the development of top-emitting OLEDs, that is, OLEDs that emit light from the top surface of devices, the requirement of transparent is unnecessary for the substrates of display devices.[7,8] However, high gases barrier and thermal and dimensional stability are demanded for the substrates. The organic materials in OLEDs are very sensitivity to moisture and oxygen which cause reliability problems.[9,10] Moisture and oxygen from the external environment easily oxidize and crystalize organic materials which lead to the formation of dark spots.[11,12] Hence, a substrate with high gases barrier properties is required to protect the device from atmospheric environment and to increase the lifetime of the device. In addition, polymer substrates are usually exposed to high temperatures during the manufacturing processes of OLEDs.[13,14] For instance, in the fabrication of active matrix organic light-emitting display devices, the processing temperature of the flexible plastic substrates is even higher than 300 °C.[15] The high dimensional stability of substrates is advantageous for making dimensionally stable designs for devices.[16] Generally, high heat resistance ($T_g > 300$ °C) and low coefficient of thermal expansion (CTE < 20 ppm K^{-1}) are demanded for the polymer substrates.[17,18] However, most of the used polymer substrates, such as polyethylene terephthalate,[19] polyethylene naphthalate,[20] and polycarbonate,[21] typically have low heat resistance ($T_g < 200$ °C) and high coefficients of thermal expansion (20–80 ppm K^{-1}).[22] These characteristics bring with them challenges in overlay registration during device fabrication. Hence, polymers substrates with excellent thermal and dimensional stability as well as high gases barrier are greatly important for the application in flexible OLEDs.

Additional Supporting Information may be found in the online version of this article.

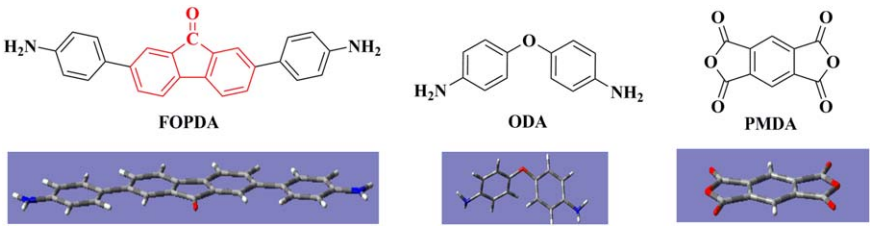

FIGURE 1 The chemical structure and stereo view of the lowest energy conformation of FOPDA, ODA and PMDA. [Color figure can be viewed at wileyonlinelibrary.com]

Polyimides (PIs) have been considered as one of the most promising candidates for flexible substrates of organic electronics devices, because of their excellent thermal and dimensional stability, solvent and chemical resistance, and electrical and mechanical properties.[1,23,24] However, the poor barrier properties of PIs have limited their application in OLEDs flexible substrates. Currently, the most widely used methods to improve the barrier properties of PIs are surface coating and preparation of nanocomposites, such as the use of atomic layer deposition or magnetron sputtering process to fabricate barrier layer on the polyimides substrate, or introducing inorganic particle into the PIs matrix to form nanocomposites.[25–28] However, these modification processes are usually complicated and high cost. Noticeably, these two modification methods are based on the pristine PIs matrix. Hence, improving the barrier properties of the pristine PIs matrix is considered as an effective route to simplify the modification processes and reduce costs.

Structure modification is usually adopted to synthesize PIs with desired properties, such as improved thermal stability, optical properties, solubility, and so on.[29–32] However, altering chemical structures to prepare intrinsic high-barrier polyimides was rarely reported in the literatures. In this work, a novel fluorenone groups-containing diamine monomer (2,7-bis(4-aminophenyl)-9H-fluoren-9-one [FOPDA]) with special rigid planar molecular structure was designed and synthesized through Suzuki coupling reaction. Then, a novel polyimide (FOPPI) derived from FOPDA and pyromellitic dianhydride (PMDA) was successfully prepared. The chemical structure and stereo view of the lowest energy conformation of FOPDA is shown in Figure 1. It can be seen that the fluorenone moiety (as shown in the red circle) in FOPDA induces a planar and relatively larger ring in the backbone, and the FOPDA shows a highly planar molecular structure, which can increase the rigidity and regularity of polymer chains. This structural characteristic is expected to increase packing density of polymer chain, thus improve the barrier properties. In addition, the rigid planar backbone structure is expected to maintain a relatively high glass transition temperature (T_g), excellent thermal and dimensional stability, and mechanical properties of the polymer. The barrier properties, thermal and mechanical properties of the polyimide are investigated in detail. Furthermore, to clarify the barrier mechanism, a contrastive study of FOPPI and analogous polyimide (Kapton) derived from 4,4′-oxydianiline (ODA) and PMDA was performed using wide angle X-ray diffractograms (WAXD), positron annihilation lifetime spectroscopy (PALS), and molecular dynamics simulations.

EXPERIMENTAL

Materials

2,7-Dibromo-9H-fluoren-9-one, tetrakis (triphenyl-phosphine) palladium ($Pd(PPh_3)_4$), (4-aminophenyl) boronic acid hydrochloride, potassium carbonate, aliquat 336 (tricaprylylmethylammonium chloride), and ODA were purchased from Alfa-Aesar company and used without further purification. PMDA was purchased from Alfa-Aesar Company and dried in a vacuum oven at 110 °C for 6 h before use. Analytical grade dimethyl formamide (DMF) was purified by distillation under an inert nitrogen atmosphere. All other reagents and solvents were purchased as analytical grade from the National Pharmaceutical Group Chemical Reagent Co., Ltd. and were used without further purification.

Measurements

Nuclear magnetic resonance (NMR) spectra were measured on a Bruker AVANCE AV 400 spectrometer in deuterated dimethyl sulfoxide (DMSO) using tetramethylsilane as the internal reference. Elemental analysis was carried out on a CHNS Elemental Analyzer. Mass spectra were measured on a Thermo EI mass spectrometer (DSQ II). Infrared spectra were recorded by a BRUKER TENSOR 27 Fourier-transform infrared (FT-IR) spectrometer. The diamine monomer was measured by using KBr pellets, and the PI film was tested through ATR mode. The molecular mass of the polyamic acid was determined by gel permeation chromatography multiangle laser light scattering (GPC-MALLS) system (Wyatt Technology Corporation) using DMF as eluent at flow rate of 1 mL min^{-1} at 50 °C. Thermogravimetric analyses (TGA) were performed using a TA thermal analyzer (Q50) under N_2 (flowing rate of 40 mL min^{-1}) in the temperature range from 40 to 900 °C with a heating rates of 10 °C min^{-1} for diamine monomer and 20 °C min^{-1} for polyimide. Differential scanning calorimetry (DSC) curves were obtained with a TA thermal analyzer (Q20). A heating rate of 10 °C min^{-1} from 20 to 300 °C under flowing nitrogen was performed. The T_g of the FOPDA was taken from the second heating trace after rapid cooling from 300 °C at a cooling rate of 10 °C min^{-1}. The midpoints of the transitions in the heat capacity were regarded as T_g value. The dynamic mechanical (DMA) spectra of the samples were obtained through a TA dynamic mechanical analyzer (DMA Q800) under N_2 (flowing

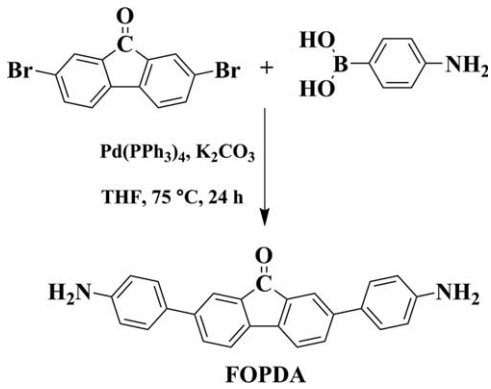

SCHEME 1 Synthesis routes of FOPDA.

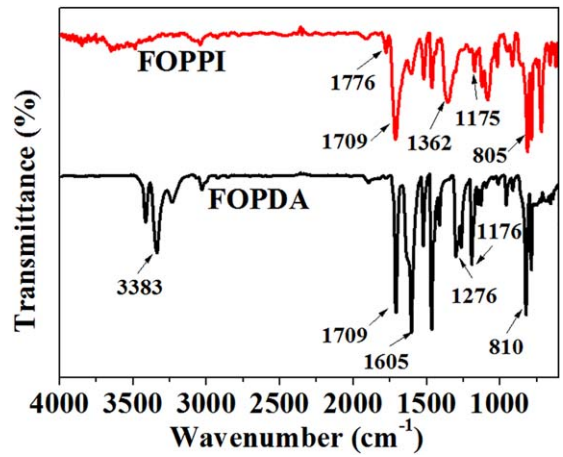

FIGURE 3 FT-IR spectra of FOPDA and FOPPI. [Color figure can be viewed at wileyonlinelibrary.com]

rate of 40 mL min^{-1}). The specimens were analyzed in tensile mode at a constant frequency of 1 Hz and a temperature range from 50 to 450 °C at a heating rate of 5 °C min^{-1}. Thermal mechanical analysis (TMA) was used to study the thermal coefficient of expansion (CTE) of the film with a heating rate of 5 °C min^{-1} from 40 to 400 °C by TMA Q400 instrument. The mechanical properties of thin films were measured with SANS CMT6103 instrument (Shenzhen, China) according to Standard GB/T16421-1996. The samples were cut from 35–50 μm thick sheet with size of 10 mm × 100 mm, and the jaw separation was 50 mm. The jaw speed was first set to 2 mm min^{-1}. When elongation reached 1 mm, the jaw speed was changed to 20 mm min^{-1}. WAXD were recorded by a Rigaku Ultima IV X-ray diffractometer using a Cu Kα radiation. The oxygen permeability of a PI film was measured by MOCON (Minneapolis, MN), in accordance with ASTM-D 3985, using an Oxtran 2/21 ML instrument at 23 °C and 0% RH. The moisture vapor permeability was measured using the model PERMATRAN-W 3/33 of the

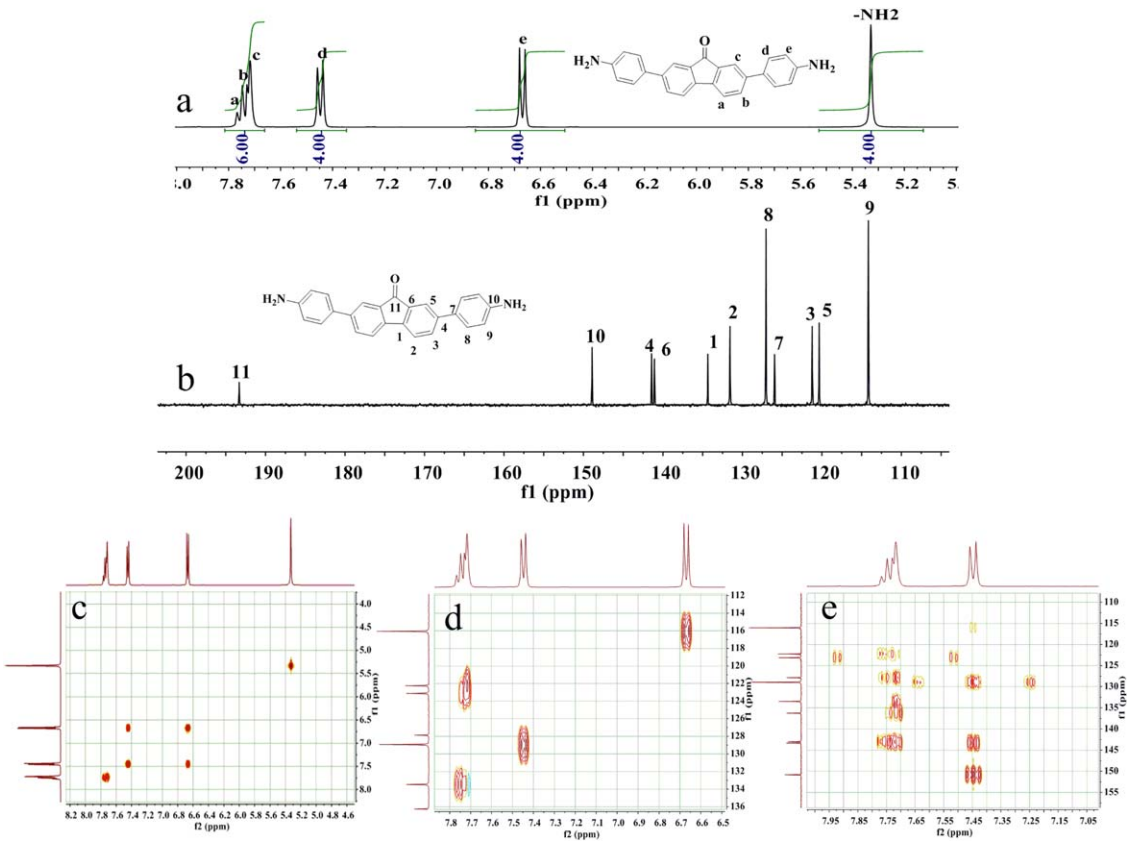

FIGURE 2 (a) ^{1}H NMR, (b) ^{13}C NMR, (c) H-H COSY, (d) C-H QC, and (e) C-H BC spectra of FOPDA in DMSO-d_6. [Color figure can be viewed at wileyonlinelibrary.com]

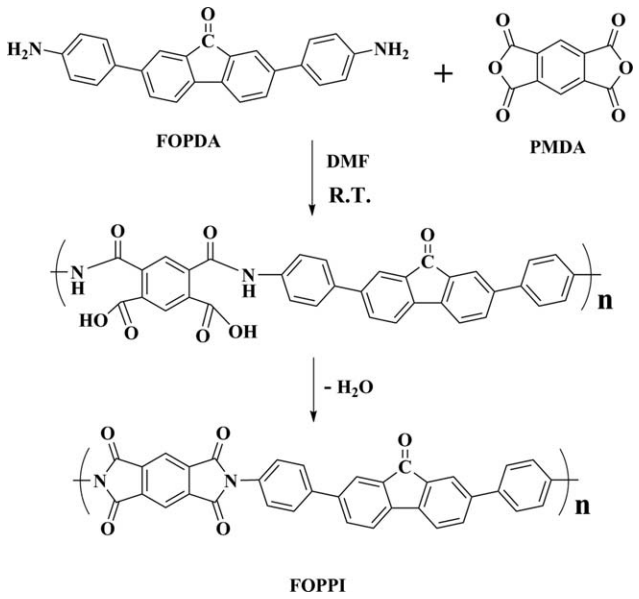

SCHEME 2 Synthesis routes of FOPPI.

Mocon Corporation (USA) at 90% RH and 37.8 °C according to ASTM F-1249. The specimen was fixed on an aluminum foil with the film testing area of 5 cm^2. For each polyimide, five samples were measured and the median value was reported. The morphology of the surface of polyimide was studied using atomic force microscopy (AFM) system (Bruker, Model Multimode 8, Germany). UV-vis absorption spectrum (UV) was recorded on a Hitachi UV-vis spectrophotometer (U-3900). The film density was measured by a density balance (Mirage SD-200 L, Japan) with an accuracy of 0.1 mg.

Positron lifetime measurements were performed using a fast–fast coincidence system. Two identical samples with dimension of 10 × 10 × 1.5 mm^3 were sandwiched between a ^{22}Na positron source with intensity of about 7 × 10^5 Bq. When the ^{22}Na nuclei emits a positron, it also emits a 1.28 MeV γ-ray simultaneously (within a few picoseconds). The positron lifetime is then determined by the time difference between the emission of the birth gamma ray (1.28 MeV) and the annihilation photon. The time resolution of the lifetime spectrometer is about 220 ps in full-width at half maximum. Totally, 4096 channels with a channel width of 12.6 ps were used to collect the positron lifetime spectrum. The PATFIT program was used to decompose the lifetime spectrum into several exponential components after background subtraction and source correction. The source components (360 ps/16.88%, 1.18 ns/0.95%) were determined using several reference samples such as Si and Al single crystals. The variance of the fit was ~1.1.

Molecular Simulation

Molecular simulations of FOPDA, PMDA, and ODA were carried out with the Gaussian 09 (revision E.09) program. Equilibrium ground state geometry of the monomers was optimized by the density functional theory (DFT) at the B3LYP level (Beckes-style three-parameter DFT using the Lee-Yang-Parr correlation functional) with the 6-31 G(d) basic set.

To understand the structural differences at molecular level, Materials Studio 7.0 from Accelrys was used for molecular dynamics simulations of polymers. Repeat units and polymer chains of FOPPI and Kapton were constructed using the "Build" function. For constructing the polymer, 25 repeat units were used with amino group as the initiator and terminator. Five polymer chains were used for the amorphous cell construction. Besides, polymer chains consisting of 10 repeat units were also constructed to discuss the single chain morphology. Isotactic polymer configuration with random torsion and head-to-tail orientation were assumed for simulating the polymer chains. The molecular chains were optimized for geometry and minimized before amorphous cell construction. To simulate the dense polyimide membranes, the amorphous cell module of FOPPI and Kapton was used for constructing a polymeric periodic cell based on COMPASS (condensed-phase optimized molecular potentials for atomistic simulation studies) force field calculations at 298 K and reduced densities of 0.2 $g{\cdot}cm^{-3}$. The geometry of the configuration is allowed to be optimized following the construction of the amorphous cell. Then, the optimized cells were compressed by using isothermal-isobaric (NPT) ensemble dynamics at pressures of 0.0001 GPa with a step time of 1.0 fs and a dynamics time of 1000 ps. Afterward, the system was relaxed by subjecting them to a series of anneal dynamics and stage wise equilibration procedure. The anneal dynamics consisted of 10 anneal cycles from 300 to 1000 K with 14 heating ramps per cycle. In the next step, the systems were dynamically equilibrated in NPT and canonical (NVT) ensemble at a temperature of 298 K. The step time of 1.0 fs and a dynamics time of 500 ps were used. The free volume and occupied volume of each amorphous polyimides were calculated using the Connolly task. Connolly radii that correspond to the kinetic diameters of H_2O and O_2 molecules were used. The simulated fractional free volumes (FFV) of the polyimides are dependent on the chosen Connolly radius since these are used as the probe particles.[33–36]

TABLE 1 Thermal Properties of the FOPPI

Polymer	T_g (°C)	$T_{d5\%}$ (°C)	$T_{d10\%}$ (°C)	*CET*[a] (ppm K^{-1})	Char Yield[b] (wt %)
FOPPI	420	607	632	1.28	72

[a] CTE within the range of 50–200 °C.

[b] Residual weight percentage at 800 °C in nitrogen.

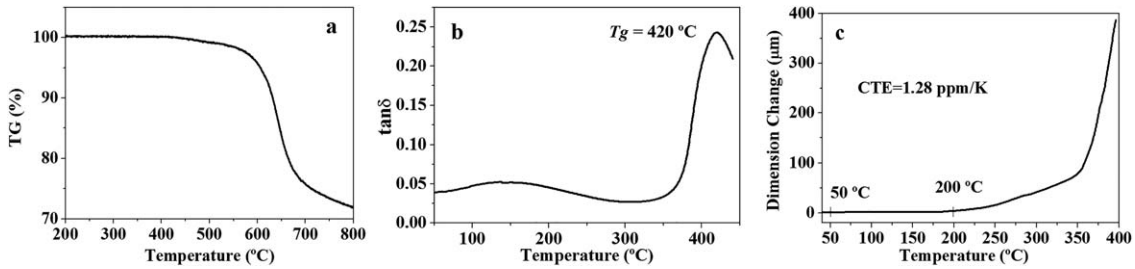

FIGURE 4 (a) TGA, (b) DMA, and (c) TMA curves of the FOPPI.

TABLE 2 Mechanical Properties of the PI Films

PI	Tensile Strength (MPa)	Tensile Modulus (GPa)
Kapton	120.6 ± 2.5	2.3 ± 0.2
FOPPI	150.8 ± 2.2	3.7 ± 0.3

Synthesis of FOPDA

2,7-Dibromo-9H-fluoren-9-one (10.140 g, 0.03 mol) and 4-aminophenylboronic acid hydrochloride (12.138 g, 0.07 mol) were dissolved in THF (600 mL) and mixed in a flask. Then, 2 M aqueous K_2CO_3 solution (105 mL) and 15 drops of Aliquat336 were added into the above mixture. The mixture was stirred for 1 h under argon at room temperature. $Pd(PPh_3)_4$ catalyst (catalytic amount) was subsequently added as a catalyst, and the reaction mixture was stirred at 75 °C for 24 h. After cooling down to room temperature, the product was concentrated and purified by silica-gel column chromatography using dichloromethane.

Yield of the product was about 82%. IR (KBr pellet, cm^{-1}): 3383 (N—H stretching), 1605 (δ N—H), 1709 (C═O stretching), 1276 (C—N stretching), 1176–810 (δ Ar—H). ^{1}H NMR (400 MHz, DMSO-d_6, δ, ppm): 7.74 (dd, J = 13.6, 6.5 Hz, 6H), 7.45 (d, J = 8.4 Hz, 4H), 6.67 (d, J = 8.5 Hz, 4H), 5.33 (s, 4H). ^{13}C NMR (101 MHz, DMSO-d_6, δ, ppm): 193.31, 148.91, 141.42, 141.07, 134.35, 131.56, 127.03, 125.96, 121.22, 120.34, 114.15. MS (EI, m/z): 362 ($[M]^+$, calcd for $C_{25}H_{18}N_2O$, 362.14). Anal. Calcd for $C_{25}H_{18}N_2O$: C 82.85, H 5.01, N 7.73; found: C 83.52, H 5.06, N 7.80.

Synthesis of PIs

The polyimide films were fabricated by a conventional two-step method. First, PMDA (0.2181 g, 1 mmol) was added into a solution of FOPDA (0.3624 g, 1 mmol) in 10 mL of purified DMF with continuous stirring, achieving a solid content of approximately 6 wt %. The above mixture was stirred at room temperature under argon for about 8 h to form a viscous poly(amic acid) (PAA) solution. Subsequently, the PAA solution was uniformly coated on a clean and dry glass plate with a controlled film thickness, and then thermally imidized in a vacuum oven with the temperature program of 100 °C (1 h)/200 °C (1 h)/300 °C (1 h)/430 °C (1.5 h) to produce polyimide film (FOPPI). The film was removed from the glass substrate after the oven cooled down to room temperature. IR(ATR, cm^{-1}): 1776 and 1709 (C═O stretching), 1362 (C—N stretching), 1175–805 (δ Ar—H). The Kapton film was prepared by the reaction of equal molar amounts of ODA and PMDA through a similar preparation process.

RESULTS AND DISCUSSION

Synthesis and Characterization of FOPDA

The FOPDA was obtained by the Suzuki coupling reaction of 2,7-dibromo-9H-fluoren-9-one with 4-aminophenylboronic acid as shown in Scheme 1. The structural analysis of the FOPDA was carried out by NMR, mass spectra, FTIR, and elemental analysis. The ^{1}H and ^{13}C NMR spectra of FOPDA are shown in Figure 2(a,b), respectively. Assignments of each carbon and proton were assisted by the two-dimensional (2D) H—H COSY, C—H QC and C—H BC NMR spectra, as shown in Figure 2(c–e). The FTIR and mass spectrum of FOPDA are shown in Figure 3 and Supporting Information Figure S1, respectively. The results of NMR, FTIR, and mass spectra were in agreement with the proposed molecular structure of FOPDA, as shown in Scheme 1. The data from elemental analysis were consistent with the calculated values, as described in Experimental section. All the results indicated that the diamine FOPDA were successfully synthesized by the Suzuki coupling reaction.

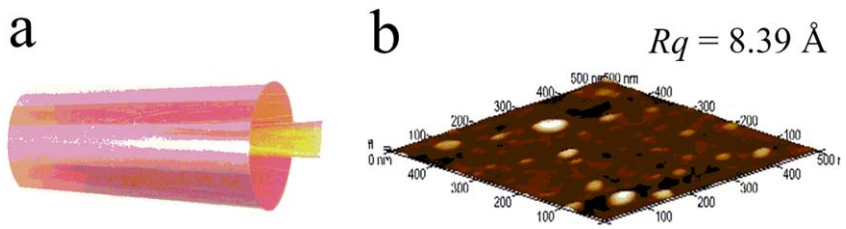

FIGURE 5 (a) Photo image of the flexible FOPPI film; (b) a typical AFM image of the FOPPI film surface. [Color figure can be viewed at wileyonlinelibrary.com]

TABLE 3 Barrier Properties FOPPI and Kapton Films

PI	WVP g mil (m^2 day) $^{-1}$	OP cm^3 mil (m^2 day) $^{-1}$	WVTR[a] g (m^2 day)$^{-1}$	OTR[b] cm^3 (m^2 day) $^{-1}$
Kapton	114.5 ± 2.1	330.7 ± 2.5	38.8 ± 0.7	112.0 ± 0.8
FOPPI	8.7 ± 0.4	9.5 ± 0.3	2.9 ± 0.1	3.2 ± 0.1

[a] WVTR was measured for 75 μm film at 37.8 °C and 90% RH.

[b] OTR was measured for 75 μm film at 23 °C and 0% RH.

The thermal properties of FOPDA were evaluated by TGA and DSC, and the corresponding data are summarized in Supporting Information Table S1. The DSC and TGA curves of FOPDA are shown in Supporting Information Figures S2 and S3, respectively. The melting temperature (T_m) and T_g of FOPDA was about 272 °C and 202 °C, respectively. The 5% and 10% weight-loss temperatures in nitrogen were 343 °C and 370 °C, respectively. These results revealed that FOPDA presented good thermal stability, which was attributed to the rigid structure.

Synthesis and Characterization of FOPPI

The polyimide FOPPI was prepared through a conventional two-step procedure by the reaction of equal molar amounts of diamine FOPDA with PMDA in DMF to form precursor PAAs, followed by thermal cyclodehydration, as shown in Scheme 2. The weight average molecular weight (M_w) and the dispersity (PDI) of the resultant PAA estimated from GPC were 8.6×10^4 and 1.73, respectively. The PAA was soluble in common polar solvents such as *N*-methylpyrroli-done, dimethyl acetamide, DMSO, DMF, and tetrahydrofuran (THF). The formation of polyimide was confirmed by FT-IR spectra in Figure 3. Compared with the spectrum of FOPDA, the characteristic absorption at 3383 cm^{-1} (N—H stretching) and 1605 cm^{-1} (δ N—H) disappeared in the spectrum of polyimide FOPPI. Meanwhile, the characteristic absorption peaks of the imide group at 1776 cm^{-1} (asymmetrical stretching of carbonyl) and 1709 cm^{-1} (symmetrical stretching of carbonyl), and the C—N bond at around 1362 cm^{-1} were clearly shown. These results indicated the successful reaction between FOPDA and PMDA, and the complete imidization reaction of the PAA.

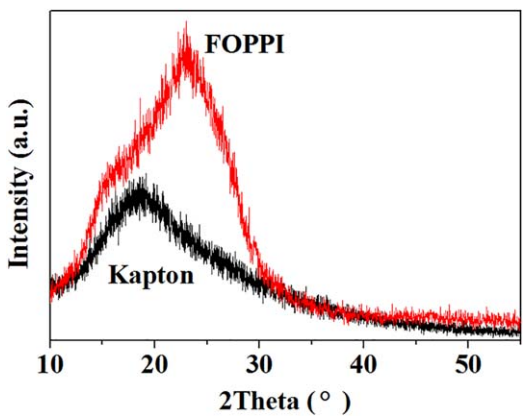

FIGURE 6 WAXD curves of FOPPI and Kapton films. [Color figure can be viewed at wileyonlinelibrary.com]

The thermal properties of the polyimide were investigated by TGA, DMA, and TMA and the analysis results are summarized in Table 1. The 5% and 10% weight-loss temperatures ($T_{d5\%}$ and $T_{d10\%}$) of the FOPPI in nitrogen were as high as 607 °C and 632 °C, respectively [Fig. 4(a)]. The amount of carbonized residue (char yield) in nitrogen atmosphere was more than 70% at 800 °C. The T_g of FOPPI was measured by DMA [Fig. 4(b)]. The T_g values was 420 °C. TMA was used to analyze the CTE of the FOPPI and the CTE value was 1.28 ppm K^{-1} within the temperature range from 50 to 200 °C [Fig. 4(c)]. The thermal stability, dimensional stability, and T_g of the FOPPI are much higher than those of the commercial polymers or other reported aromatic polymers, which allow it to undergo processing temperatures in excess of 400 °C. For example, the isothermal weight loss of the FOPPI at 450 °C for 30 min is low as 2% (Supporting Information Fig. S4). These excellent thermal properties of the FOPPI could be attributed to the existence of rigid planar moieties in the polymer backbone.[37,38]

Mechanical properties of the polymer membrane are also an important parameter for flexible substrate. As shown in Table 2, FOPPI showed excellent mechanical properties with the tensile strength of 150.8 MPa and tensile modulus of 3.7 GPa, which are much higher than those of Kapton film. Figure 5(a) showed a rolled FOPPI film, which demonstrated the good flexibility of the film. The optical property of the polyimide film has been investigated by UV-vis spectroscopy. The transmission UV-vis spectrum of the polyimide film observed in the visible region showed the cut off wavelength (λ_0) of 449 nm (Supporting Information Fig. S5). This polyimide film was in light-color with good transparency (more than 85% transmittance in the visible region). The polyimide was insoluble in common polar solvents. AFM investigation revealed that the film had smooth and compact surface with a surface roughness (R_q) of 8.39 Å [Fig. 5(b)]. Low surface roughness (average surface roughness < 5 nm) of polymer substrates is essential to ensure the integrity of subsequent surface layers including barrier and conductive layers.[17] The high T_g, outstanding thermal and dimensional stability, and excellent mechanical properties of the FOPPI are expected to meet the requirements of heat resistance, dimensional

TABLE 4 Physical Properties of the FOPPI and Kapton

Polymers	Density (g cm^{-3})	2θ (°)	*d*-Spacing (Å)
Kapton	1.4246	19.08	4.65
FOPPI	1.4956	23.07	3.85

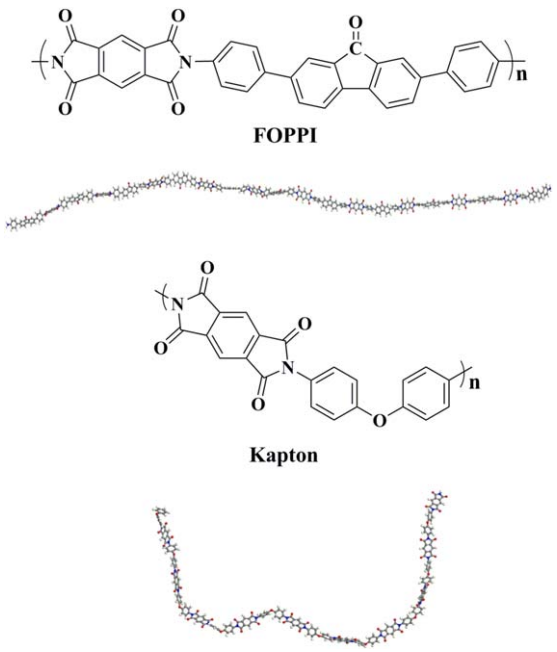

FIGURE 7 The stereo view of the lowest energy conformation of FOPPI and Kapton chains. [Color figure can be viewed at wileyonlinelibrary.com]

stability and high processing temperatures (higher than 400 °C) as flexible substrates for organic electronics devices.

Barrier Properties

As for barrier properties study, the FOPPI is compared with a structurally related polyimide (Kapton) derived from diamine ODA and PMDA. Herein, the ODA has a twist at the ether linkage and the two benzene rings are nonplanar (Fig. 1). The detail data for barrier properties of FOPPI and Kapton are summarized in Table 3. It can be seen that the oxygen transmission rate (OTR) and water vapor transmission rate (WVTR) of FOPPI were low to 3.2 $cm^3 \cdot m^{-2} \cdot day^{-1}$ and 2.9 $g \cdot m^{-2} \cdot day^{-1}$, respectively. Compared with Kapton, the OTR and WVTR of FOPPI were decreased by 97% and 92%,

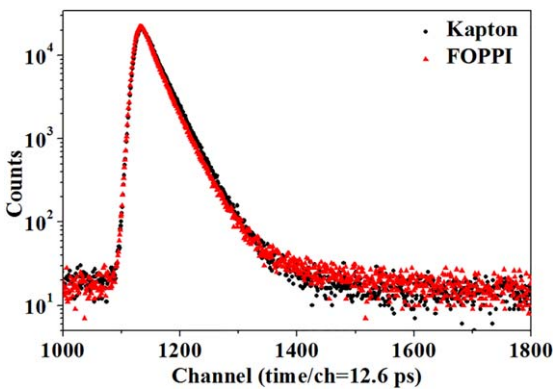

FIGURE 8 Positron lifetime spectra measured for the FOPPI and Kapton films. [Color figure can be viewed at wileyonlinelibrary.com]

TABLE 5 The Analyzed Data for the Positron Lifetime in the Kapton and FOPPI Films

PI	τ_1 (ns)	I_1 (%)	τ_2 (ns)	I_2 (%)	R (Å)	V_{f2} (Å^3)	FFV (%)
Kapton	0.17	13.0	0.38	86.8	2.6037	73.90	11.55
FOPPI	0.15	24.3	0.35	74.9	2.2633	48.54	6.54

respectively. The barrier properties of FOPPI are much better than those of Kapton film and the reported intrinsic PIs.[17,39]

Mechanisms Studies of Barrier Properties

Crystallinity Analysis

To clarify the barrier mechanism of FOPPI, we go further into the chemical structure and morphology of the polyimide films. The WAXD scattering spectra of FOPPI and Kapton are shown in Figure 6. It can be seen that the FOPPI displayed a relatively sharp and intensive reflection peak, indicating the higher crystallinity of the FOPPI than that of Kapton. The higher crystallinity of the FOPPI was mainly due to the high planarity and regularity of the polymer backbone structure. It is reported that polymer crystals are impermeable for most low-molecular-weight substances, while the amorphous phase is the only phase available for permeation of these substances.[40,41] Therefore, the permeating molecules in the FOPPI have to circumvent the crystallite regions, resulting in a more tortuous diffusive pathway than that in the Kapton. As a result, the barrier properties of the FOPPI are significantly improved.

The positions of the intensity maximum in the bands of the WAXD scattering spectra are considered as the most probable intersegmental distance (d-spacing) between the polymer chains. Kapton presented the diffraction peak at $2\theta = 19.08°$ with the d-spacing of 4.65 Å (Table 4), while the FOPPI exhibited the diffraction peak at $2\theta = 23.07°$ with the smaller d-spacing of 3.85 Å. The density values of the polymer films are shown in Table 4. The density of the FOPPI film was 1.4956 g cm^{-3}, with an increase of 5% compared with that of Kapton. The low intersegmental distance and higher density of the FOPPI indicated its high degree of chain packing, which are resulted from the planar and regular polymer backbone.

To understand the ability of chains packing, the chain morphologies of FOPPI and Kapton were studied using Materials Studio software. Figure 7 shows the single chain morphologies of FOPPI and Kapton containing 10 repeat units at the completely extended state. Although there is a deviation between the morphologies and real conformation in our membranes, it is still valuable for the qualitative discussion to correlate membrane performance with their chemical structures. From Figure 7, it can be seen that the FOPPI had a much extended chain conformation, indicating the higher rigidity and regularity of the polymer backbone; while Kapton exhibited curving chain morphology, illuminating the more flexibility and disorder of the polymer backbone. The special planar molecule structure and extended chain conformation of FOPPI were beneficial to increasing the degree of chain packing and reducing free volume of the polymer.[37,42] The results of crystallinity, density and intersegmental

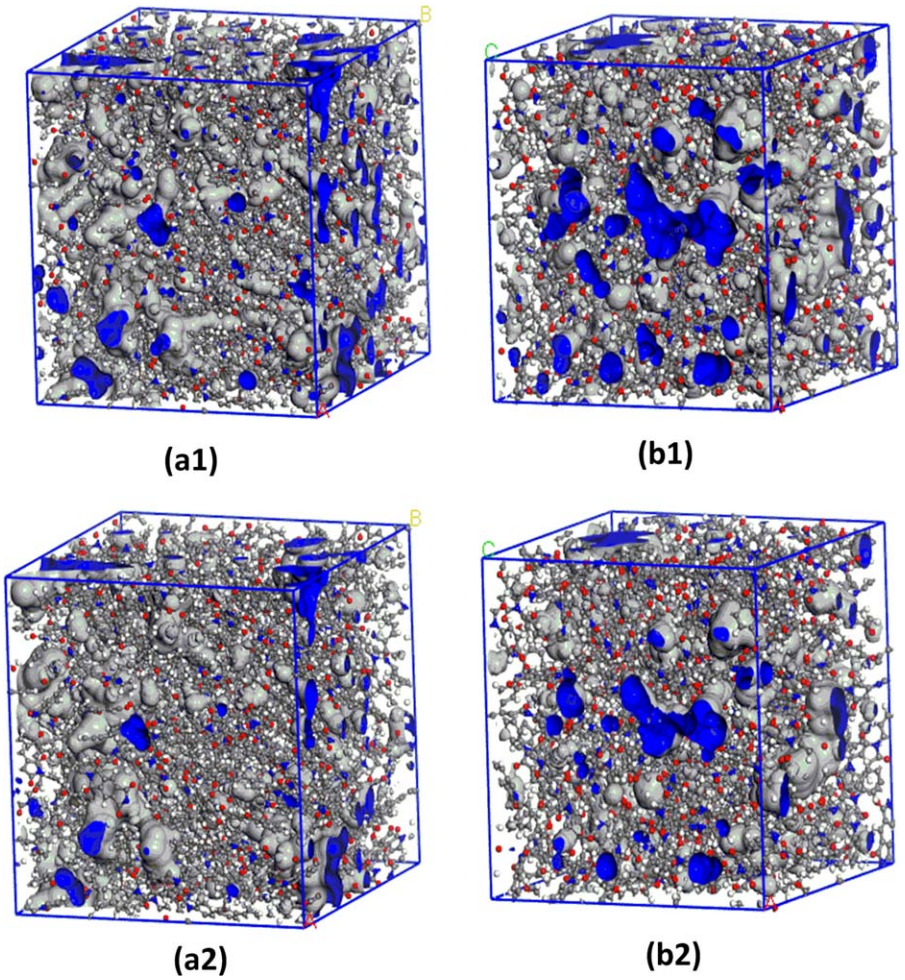

FIGURE 9 (a1) (a2) Simulated amorphous cell containing FOPPI chains; (b1) (b2) simulated amorphous cell containing Kapton chains (grey: Van der Waals surface; blue: Connolly surface; a1 and b1: probe radius of 1.325 Å; a2 and b2: probe radius of 1.73 Å). [Color figure can be viewed at wileyonlinelibrary.com]

distance confirmed the differences of chains packing ability in FOPPI and Kapton.

Additionally, it can be seen from the chain morphologies, the polymer chains of FOPPI with fluorenone moiety in backbone were more rigid than that of Kapton with ether linkage. Thus, the chain mobility of FOPPI was poorer than that of Kapton. The channel formation for the molecule to permeate is dependent on the mobility of the polymer chains.[36] Hence, the decreased chain mobility in the FOPPI decreased the extent of channel formation for gas diffusion, leading to the improvement in barrier properties.

Free Volume Analysis

Positron Annihilation Lifetime Spectroscopy

PALS is a useful method for studying the free volume of polymer materials.[43–45] The positron lifetime spectra measured for FOPPI and Kapton films are shown in Figure 8. A detailed analysis of the lifetime spectra of FOPPI and Kapton are summarized in Table 5. There were two exponential decay components (τ_1 and τ_2) for the FOPPI and Kapton film. Each lifetime had a corresponding intensity (I) relating to the number of annihilations occurring at a particular lifetime. The shortest lifetime τ_1 was 0.15 ns for FOPPI and 0.17 ns for Kapton, which is due to the *p*-Ps lifetime and the free annihilation lifetime of the positrons. The second lifetime component τ_2 is attributed to positron annihilation in the amorphous region, particularly in the free volume holes, which were 0.35 ns for FOPPI and 0.38 ns for Kapton. It can be seen that these two polyimides showed no long-lifetime component τ_3, which is attributed to pick-off annihilation of *o*-Ps at holes in the amorphous phase.

Jean and coworkers[46] have developed a newly modified correlation equation between the second-component positron

TABLE 6 Simulated FFV of PI Films

PI	FFV (H_2O,%)[a]	FFV (O_2,%)[b]
Kapton	15.80	10.48
FOPPI	14.52	8.98

[a] Simulated FFV based on a Connolly radius of 1.325 Å.
[b] Simulated FFV based on a Connolly radius of 1.73 Å.

lifetime (τ_2) and free volume radius using PALS, which is useful in the determination of the free-volume size in polymeric materials, where no *o*-Ps component is observed. The correlation equation has been established as follow:

$$\tau_2 = 0.260 \times \left[1 - \frac{R}{R+3.823} + \frac{1}{2\pi}\sin\left(\frac{2\pi R}{R+3.823}\right)\right]^{-1} \quad (1)$$

where τ_2 and the mean free-volume radius (R) are expressed in the units of nanoseconds and angstroms, respectively. Equation 1 is applicable well to τ_2 values from 0.260 to 0.60 ns or the hole radius up to 5 Å. The mean free-volume radius (R) can be computed using Eq. 1.

As there are only two lifetime components, the intensity of the second component I_2 can be a reflection of the relative number of free volume holes. The cavities are assumed to be spherical, so the mean free volume size (V_{f2}) of a cavity and the relative FFV can be given by eqs 2 and 3, respectively.

$$V_{f2} = \frac{4\pi R^3}{3} \quad (2)$$

$$\mathrm{FFV} = CI_2V_{f2} \quad (3)$$

where V_{f2} and I_2 are expressed in the units of $Å^3$ and %, respectively. C is an arbitrarily chosen scaling factor for a spherical cavity and depends on the chemical composition of the void walls and has typically a value of 0.0018.[47,48] The small changes in the chemistry of these polymers will not significantly influence the ionization potential of the polymer and hence will have only a small effect on the values measured. However, the values should be considered as relative rather than absolute.

The calculated free volume radius, free volume size, and the relative FFV of Kapton and FOPPI are summarized in Table 5. The mean free volume size of 73.90 $Å^3$ in Kapton film was decreased to 48.54 $Å^3$ in FOPPI film. The corresponding relative FFV of 11.55% in Kapton film was also decreased to 6.54% in FOPPI. The small free volume size and relative FFV of the FOPPI were in accordance with the results of low intersegmental distance, high density, and high barrier discussed above.

Molecular Simulations

To understand the barrier properties at molecular level, molecular dynamics simulations of FOPPI and Kapton were performed using Materials Studio software. To mimic the packing of polyimides chains in dense membranes, amorphous cells packed with the respective polymers were simulated in our work. The Connolly algorithm was used to determine the occupied and free volume within the amorphous cells. Two Connolly radii, each corresponding to the kinetic diameters of H_2O and O_2 were used to estimate the FFV of polymer. The cacluated FFV by H_2O and O_2 Connolly radii presented the FFV avaliable for the diffusion of H_2O and O_2 molecules, respectively. The simulated amorphous cells of FOPPI and Kapton are depicted in Figure 9. The FOPPI model showed smaller regions of free pace (as shown in blue) than that of Kapton film. To illustrate quantitatively, the FFV of the FOPPI and Kapton are listed in Table 6. Referring to Table 6, the H_2O accessible FFV and O_2 accessible FFV of the FOPPI are much smaller than those of Kapton, which is in agreement with the FFV results estimated from PALS. It is worth to notice that the crystallinity had not been taken into account in the calculation of free volume for FOPPI. Hence, the calculated FFV values from molecular simulations were higher than the true H_2O and O_2 accessible FFV values. This is because that the polymer crystals are impermeable for H_2O and O_2 molecules. The smaller FFV of FOPPI is mainly due to the rigid planar backbone structure and extended chain conformation of FOPPI, which is beneficial to efficient packing of the polymer chains. The efficient chain packing results in relatively less open and accessible cavities within the polymeric matrix, thus leading to a lower gas permeability. As a result, the FOPPI exhibited better barrier properties compared with Kapton.

CONCLUSIONS

An intrinsic high-barrier and thermally stable polyimide (FOPPI) was successfully prepared by the reaction of PMDA and a novel diamine containing rigid planar moiety. The polyimide showed outstanding barrier properties with the oxygen and water vapor transmission rate as low as 3.2 $cm^3 \cdot m^{-2} \cdot day^{-1}$ and 2.9 $g \cdot m^{-2} \cdot day^{-1}$, respectively. The excellent barrier properties were mainly attributed to the crystallinity, high chain rigidity, and low free volume of the FOPPI, which was resulted from the rigid planar structure. Furthermore, FOPPI exhibited high T_gs and weight-loss temperatures, as well as excellent mechanical properties. The excellent comprehensive performances made the polyimide suitable candidates for flexible electronics encapsulation application.

ACKNOWLEDGMENTS

This work was supported by the National Natural Science Foundation of China (no. 51603066, 11372108), the China Postdoctoral Science Foundation (no. 2015M580692), the Science Research Project of Hunan Provincial Department of Education (no. 16B068), the Natural Science Foundation of Hunan Province (no. 2017JJ3055) and the Research Funds for Key Laboratory of Functional and High Performance Polymeric Materials of Guangdong Province (no. 20151004). The authors thank Prof. Zhiquan Chen from Hubei Nuclear Solid Physics Key Laboratory, Department of Physics, Wuhan University, for their help in the measurement of the polymer free volume.

R.EFERENCES AND NOTES

1 S. Logothetidis, *Mater. Sci. Eng. B.* **2008**, *152*, 96–104.

2 S. Kim, H. J. Kwon, S. Lee, H. Shim, Y. Chun, W. Choi, J. Kwack, D. Han, M. Song, S. Kim, S. Mohammadi, I. Kee, S. Y. Lee, *Adv. Mater.* **2011**, *23*, 3511–3516.

3 S. Ju, J. F. Li, J. Liu, P. C. Chen, Y. G. Ha, F. Ishikawa, H. Chang, C. W. Zhou, A. Facchetti, D. B. Janes, T. J. Marks, *Nano Lett.* **2008**, *8*, 997–1004.

4 M. C. Choi, J. C. Hwang, C. Kim, S. Ando, C. S. Ha, *J. Polym. Sci. Part A: Polym. Chem.* **2010**, *48*, 1806–1814.

5 P. Heremans, A. K. Tripathi, A. D. de Meux, E. C. P. Smits, B. Hou, G. Pourtois, G. H. Gelinck, *Adv. Mater.* **2016**, *28*, 4266–4282.

6 G. X. Qin, H. C. Yuan, H. J. Yang, W. D. Zhou, Z. Q. Ma, *Semicond. Sci. Technol.* **2011**, *26*, 25005–25010.

7 C. Fuchs, P. A. Will, M. Wieczorek, M. C. Gather, S. Hofmann, S. Reineke, K. Leo, R. Scholz, *Phys. Rev. B.* **2015**, *92*, 245306–245316.

8 T. Schaefer, T. Schwab, S. Lenk, M. C. Gather, *Appl. Phys. Lett.* **2015**, *107*, 110–111.

9 P. E. Burrows, G. L. Graff, M. E. Gross, P. M. Martin, M. K. Shi, M. Hall, E. Mast, C. Bonham, W. Bennett, M. B. Sullivan, *Displays* **2001**, *22*, 65–69.

10 H. Ito, W. Oka, H. Goto, H. Umeda, *Jpn. J. Appl. Phys.* **2006**, *45*, 4325–4329.

11 S. Gardonio, L. Gregoratti, P. Melpignano, L. Aballe, V. Biondo, R. Zamboni, M. Murgia, S. Caria, A. Kiskinova, *Org. Electron.* **2007**, *8*, 37–43.

12 S. F. Lim, W. Wang, S. J. Chua, *Mat. Sci. Eng. B.* **2001**, *85*, 154–159.

13 J. S. Lewis, M. S. Weaver, *Ieee J. Sel. Top Quant.* **2004**, *10*, 45–57.

14 S. K. Park, J. I. Han, W. K. Kim, M. G. Kwak, *Thin Solid Films* **2001**, *397*, 49–55.

15 J. Lewis, *Mater. Today* **2006**, *9*, 38–45.

16 B. Hekmatshoar, K. H. Cherenack, A. Z. Kattamis, K. Long, S. Wagner, J. C. Sturm, *Appl. Phys. Lett.* **2008**, *93*, 032103.

17 M. C. Choi, Y. Kim, C. S. Ha, *Prog. Polym. Sci.* **2008**, *33*, 581–630.

18 J. L. Chen, C. T. Liu, *Ieee Access.* **2013**, *1*, 150–158.

19 T. W. Kelley, P. F. Baude, C. Gerlach, D. E. Ender, D. Muyres, M. A. Haase, D. E. Vogel, S. D. Theiss, *Chem. Mater.* **2004**, *16*, 4413–4422.

20 V. Zardetto, T. M. Brown, A. Reale, A. Di Carlo, *J. Polym. Sci. Part B: Polym. Phys.* **2011**, *49*, 638–648.

21 W. A. MacDonald, M. K. Looney, D. MacKerron, R. Eveson, R. Adam, K. Hashimoto, K. Rakos, *J. Soc. Inf. Display* **2007**, *15*, 1075–1083.

22 H. Tetsuka, T. Ebina, T. Tsunoda, H. Nanjo, F. Mizukami, *Nanotechnology* **2007**, *18*, 13288–13296.

23 X. Y. Gao, L. Lin, Y. C. Liu, X. Q. Huang, *J. Disp. Technol.* **2015**, *11*, 666–669.

24 D. J. Liaw, K. L. Wang, Y. C. Huang, K. R. Lee, J. Y. Lai, C. S. Ha, *Prog. Polym. Sci.* **2012**, *37*, 907–974.

25 W. H. Koo, S. M. Jeong, S. H. Choi, H. K. Baik, S. M. Lee, S. J. Lee, *J. Phys. Chem. B.* **2004**, *108*, 18884–18889.

26 C. Charton, N. Schiller, M. Fahland, A. Hollander, A. Wedel, K. Noller, *Thin Solid Films* **2006**, *502*, 99–103.

27 M. H. Tsai, C. J. Chang, H. H. Lu, Y. F. Liao, I. H. Tseng, *Thin Solid Films* **2013**, *544*, 324–330.

28 M. H. Tsai, H. Y. Wang, H. T. Lu, I. H. Tseng, H. H. Lu, S. L. Huang, J. M. Yeh, *Thin Solid Films* **2011**, *519*, 4969–4973.

29 J. Zhao, L. Peng, Y. L. Zhu, Y. J. Song, L. J. Wang, Y. Z. Shen. *Polymer* **2016**, *91*, 118–127.

30 Y. Zhuang, J. G. Seong, Y. S. Do, W. H. Lee, M. J. Lee, M. D. Guiver, Y. M. Lee, *J. Membr. Sci.* **2016**, *504*, 55–65.

31 Y. W. Liu, C. Qian, L. J. Qu, Y. N. Wu, Y. Zhang, X. H. Wu, B. Zou, W. X. Chen, Z. Q. Chen, Z. G. Chi, S. W. Liu, X. D. Chen, J. R. Xu, *Chem. Mater.* **2015**, *27*, 6543–6549.

32 Y. W. Liu, Y. Zhang, Q. Lan, S. W. Liu, Z. X. Qin, L. H. Chen, C. Y. Zhao, Z. G. Chi, J. R. Xu, J. Economy. *Chem. Mater.* **2012**, *24*, 1212–1222.

33 B. T. Low, Y. C. Xiao, T. S. Chung. *Polymer* **2009**, *50*, 3250–3258.

34 D. Bera, P. Bandyopadhyay, S. Ghosh, S. Banerjee, V. Padmanabhan, *J. Membr. Sci.* **2015**, *474*, 20–31.

35 G. Marque, S. Neyertz, J. Verdu, V. Prunier, D. Brown, *Macromolecules* **2008**, *41*, 3349–3362.

36 S. Seethamraju, P. C. Ramamurthy, G. Madras, *Acs Appl. Mater. Inter.* **2013**, *5*, 4409–4416.

37 M. Hasegawa, T. Ishigami, J. Ishii, K. Sugiura, M. Fujii, *Eur. Polym. J.* **2003**, *49*, 3657–3672.

38 S. UrRehman, P. Li, H. W. Zhou, X. G. Zhao, G. D. Dang, C. H. Chen, *Polym. Degrad. Stabil.* **2012**, *97*, 1581–1588.

39 G. F. Sykes, A. K. Clair, *J. Appl. Polym. Sci.* **1986**, *32*, 3725–3735.

40 A. Guinault, C. Sollogoub, V. Ducruet, S. Domenek, *Eur. Polym. J.* **2012**, *48*, 779–788.

41 Y. S. Hu, A. Hiltner, E. Baer, *J. Appl. Polym. Sci.* **2005**, *98*, 1629–1642.

42 M. Hasegawa, T. Ishigami, J. Ishii, *Polymer* **2015**, *74*, 1–15.

43 D. Cangialosi, H. Schut, A. van Veen, S. J. Picken, *Macromolecules* **2003**, *36*, 142–147.

44 G. Dlubek, T. Lupke, J. Stejny, M. A. Alam, M. Arnold, *Macromolecules* **2000**, *33*, 990–996.

45 C. Dlubek, D. Bamford, O. Henschke, J. Knorr, M. A. Alam, M. Arnold, T. Lupke, *Polymer* **2001**, *42*, 5381–5388.

46 K. S. Liao, H. M. Chen, S. Awad, J. P. Yuan, W. S. Hung, K. R. Lee, J. Y. Lai, C. C. Hu, Y. C. Jean, *Macromolecules* **2011**, *44*, 6818–6826.

47 X. Hong, Y. C. Jean, H. Yang, S. S. Jordan, W. J. Koros, *Macromolecules* **1996**, *29*, 7859–7864.

48 Y. C. Jean, *Microchem. J.* **1900**, *42*, 72–102.